

Appendix A

Anthropogenic influence on recent circulation-driven Antarctic sea-ice changes*

F. Alexander Haumann^{1,2,3}, Dirk Notz¹, Hauke Schmidt¹

¹Max Planck Institute for Meteorology, Hamburg, Germany

²Environmental Physics, Institute of Biogeochemistry and Pollutant Dynamics, ETH Zürich, Zürich, Switzerland

³Center for Climate Systems Modeling, ETH Zürich, Zürich, Switzerland

Key points:

- Observed Antarctic sea ice trends could be caused by anthropogenic drivers
- A zonally asymmetric circulation change drives observed net sea-ice increase
- A zonally too symmetric circulation change in models causes sea-ice decrease

*Published in Geophysical Research Letters, 2014, volume 41, pages 84298437, doi:10.1002/2014GL061659.

Abstract

Observations reveal an increase of Antarctic sea ice over the past three decades, yet global climate models tend to simulate a sea-ice decrease for that period. Here, we combine observations with model experiments (MPI-ESM) to investigate causes for this discrepancy and for the observed sea-ice increase. Based on observations and atmospheric reanalysis, we show that on multi-decadal time scales Antarctic sea-ice changes are linked to intensified meridional winds that are caused by a zonally asymmetric lowering of the high-latitude surface pressure. In our simulations, this surface-pressure lowering is a response to a combination of anthropogenic stratospheric ozone depletion and greenhouse gas increase. Combining these two lines of argument, we infer a possible anthropogenic influence on the observed sea-ice changes. However, similar to other models, MPI-ESM simulates a surface-pressure response that is rather zonally symmetric, which explains why the simulated sea-ice response differs from observations.

A.1 Introduction

Atmospheric circulation changes around Antarctica substantially influence Antarctic sea ice. This relation emerges as an imprint of the Southern Annual Mode (SAM), the dominant mode of circulation variability in the Southern Hemisphere, on interannual sea-ice variations (Stammerjohn et al., 2008; Simpkins et al., 2012). Over the past three decades, the near-surface circulation has significantly intensified, shifting the SAM to more positive phases (Abram et al., 2014). This is most likely due to anthropogenic stratospheric ozone depletion and greenhouse-gas (GHG) increase (Lee and Feldstein, 2013; Abram et al., 2014). However, the response of Antarctic sea ice to this circulation intensification, and thus to the underlying anthropogenic forcing, is not well understood (Bitz and Polvani, 2012; Polvani and Smith, 2013; Sigmond and Fyfe, 2014). This is owing to the puzzling disagreement between observed and modeled Antarctic sea-ice trends and to a lack of process understanding concerning the influence of recent multi-decadal atmospheric circulation changes on the sea ice. We here combine observations with model simulations to address both these issues.

Satellite observations show an Antarctic sea-ice increase since the late 1970s (Comiso and Nishio, 2008), which results from strong opposing regional changes (Stammerjohn et al., 2008). The sea-ice increase in the Ross Sea since the early 1990s is related to enhanced northward ice advection due to stronger southerly winds from Antarctica, whereas advection of warmer air masses from lower latitudes causes a sea-ice decrease in that period in the West Antarctic Peninsula (WAP) region (Haumann, 2011; Holland and Kwok, 2012). These opposing regional sea-ice changes can be explained by a cyclonic circulation anomaly in the region of the Amundsen Sea Low (ASL) (Turner et al., 2009).

These observed circulation and sea-ice changes could either be caused by a change in the external forcing or simply be a manifestation of internal variability, which is of comparable magnitude to the observed trend in model simulations (Polvani and Smith, 2013; Zunz et al., 2013). A recent study by Fan et al. (2014) supports the latter suggestion by relating multi-decadal variations in temperature records to sea-ice changes. Such changes in the Antarctic surface climate show connections to the tropical Atlantic (Li et al., 2014; Simpkins et al., 2014) and Pacific (Ding et al., 2011; Schneider et al., 2012a) that alter the surface pressure in the ASL region.

In current global models, however, the recent sea-ice response seems to be dominated by changes in the external forcing. Otherwise, there would be no reason for coupled global models to consistently simulate an Antarctic sea-ice decrease over the observational period (Mahlstein et al., 2013). This simulated ice loss must hence be a direct response to increasing GHGs, stratospheric ozone depletion, and other external forcings. Bitz and Polvani (2012) and Sigmond and Fyfe (2014) explain this response by the modeled strengthening and poleward shift of the near-surface westerly winds, which enhances upwelling of warmer water in the Southern Ocean that melts the ice. These findings contradict the suggestion by Turner et al. (2009) that stratospheric ozone depletion could be the cause for the observed sea-ice changes.

Here, we further explore the possibility of a dominating external driver: Could ozone depletion and/or GHG increase cause the observed sea-ice changes if natural variability was not a sufficient explanation? To answer this question, we examine if the observed and the modeled changes in atmospheric circulation and the related sea-ice response are consistent with a primarily anthropogenic forcing. Doing so, we also gain insights that explain the disagreement between the modeled and the observed evolution of Antarctic sea ice and tropospheric circulation.

A.2 Methods, model & data

We compare model simulations to the atmospheric circulation (sea-level pressure (SLP), 10-m winds, and geopotential height) from ERA-Interim reanalysis (Dee et al., 2011) and to the observed sea-ice concentration (Meier et al., 2013a) and drift (Fowler et al., 2013a). The ERA-Interim reanalysis provides the most reliable atmospheric circulation and its changes in the southern high-latitudes among the reanalysis data (Bracegirdle and Marshall, 2012). We use the fully coupled Max Planck Institute for Meteorology Earth System Model (MPI-ESM) in its low-resolution configuration (Giorgetta et al., 2013), which contributed to the fifth Climate Model Intercomparison Project (CMIP5). The atmospheric component (ECHAM6) (Stevens et al., 2013) is run at a T63 (1.875°) horizontal resolution with 47 vertical hybrid levels reaching up to 0.01 hPa, thus resolving stratospheric changes (Schmidt et al., 2013). The ocean component (MPIOM) (Jungclaus et al., 2013) has a horizontal resolution of about 1.5° on a bipolar grid with 40 unevenly spaced vertical levels. Sea ice is implemented as a thermodynamic-dynamic model (Notz et al.,

2013). In the Arctic, MPI-ESM realistically simulates the sea-ice cover and its response to anthropogenic forcings (Notz et al., 2013). However, in the Antarctic, it underestimates the mean sea-ice extent in all seasons and considerably overestimates its natural variability over the past few decades, as do other CMIP5 models (Turner et al., 2013; Zunz et al., 2013).

We use two sets of simulations that differ in their prescribed stratospheric ozone concentration. One set uses historical GHG emissions and stratospheric ozone depletion (Experiment 1). For this set, we use the three historical simulations carried out with MPI-ESM for CMIP5, covering the period 1850–2005 (Giorgetta et al., 2012a). The evolution of GHGs and total column ozone (Cionni et al., 2011) in these simulations is shown in Figure A.1 (solid lines). A second set of three simulations (Experiment 2) is driven by the same forcings except for stratospheric ozone: We modified the forcing as such that the stratospheric ozone (mixing ratio above 150 ppb) only follows seasonal and interannual variations in the solar irradiance. Anthropogenic changes in stratospheric ozone concentration are hence excluded (Figure A.1; green dashed line). Changes in all other forcings such as solar irradiance, tropospheric ozone, and aerosols (Giorgetta et al., 2013) are identical in both experiments. These two experiments allow us to directly study MPI-ESM’s response to (1) the combined effect of GHG increase and stratospheric ozone depletion, (2) the effect of GHG increase alone, and (3) the effect of stratospheric ozone depletion alone, where the latter is estimated by examining the difference between the two experiments. In addition, we assess the mean state and internal variability in the model using a 1000-year pre-industrial (prior to 1850) control simulation with constant external forcing (Giorgetta et al., 2012b).

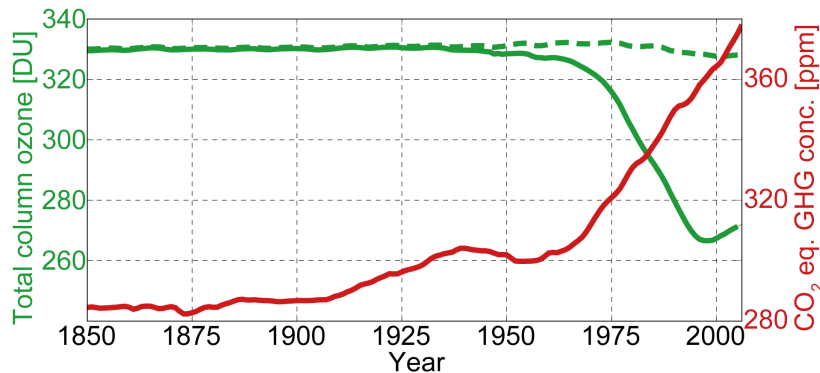


Figure A.1 External forcings of model experiments: Red: GHG forcing of Experiments 1 and 2. Green: total column ozone between 63° S and 90° S of Experiment 1 (solid) and Experiment 2 (dashed).

We analyze the ensemble mean of three realizations in each respective forcing experiment. Each of these realizations started from different initial conditions taken from the pre-industrial control simulation. We use annual means since we are interested in the net response to the forcing. Hence, we neglect possible differences in seasonal variations and trends (Simpkins et al., 2012; Holland, 2014). We calculate linear trends with a least squares regression analysis for the observational period 1979 to 2011 and, to minimize the impact of internal variability, a longer model period from 1960 to 2005 (see supplemental material for details).

A.3 Results

The annual mean near-surface wind field from the ERA-Interim reanalysis shows that the Antarctic sea ice experiences westerly winds near the ice edge (Figure A.2a), whereas most of the coastal and interior sea-ice regions experience easterly to southerly winds. The low-pressure belt around Antarctica consists of three distinct climatological SLP minima, with the ASL showing the lowest SLP (Figure A.2a). The zonal SLP gradients induced by the asymmetric distribution determine the advection of warmer air masses west of the WAP and the advection of cold continental air over the south-western Ross and Weddell Seas, influencing the sea-ice formation and export (Haumann, 2011). This zonal asymmetry intensifies between 1979 and 2011 (Figure A.2c). In particular, the low SLP in the ASL region expands and deepens significantly, leading to increased southerly winds in the western Ross Sea and increased northerly winds in the WAP region. In all other regions the westerlies strengthen. Similar asymmetric structures in the SLP trends have been reported for other reanalysis data sets, but the detailed spatial structure and the magnitude of the trends varies among them (Bromwich et al., 2011).

The meridional wind changes (Figure A.2c) go along with a sea-ice concentration increase in the Ross Sea and a decrease west of the WAP (Figure A.2e). The southerly wind anomaly in the Ross Sea, the expansion of the ASL, and the associated decrease in westerly winds in this region explain the dominating sea-ice increase in the western Ross Sea compared to the smaller increase in the eastern Ross Sea. Generally, sea ice drifts at a turning angle of roughly 20° to 40° to the wind direction (Kottmeier et al., 1992). Consequently, we show that the finding by Haumann (2011) and Holland and Kwok (2012), that ice-drift changes (Figure A.2e) are induced by wind changes (Figure A.2c), is also evident over the period 1979 to 2011. Potential inconsistencies in the drift trend (Fowler et al., 2013a; Olason and Notz, 2014) do not affect these results qualitatively (Figure A.4). The increased northward drift in the Ross Sea causes a higher sea-ice production at the coast, a higher northward advection, thus an expansion and concentration increase at the ice edge. The decrease in the WAP region is associated with the advection of warmer air masses from lower latitudes (Haumann, 2011; Holland and Kwok, 2012). The increase of the total Antarctic sea-ice area over the observational period (Comiso and Nishio, 2008) is mostly due to a large sea-ice area gain in the Ross Sea and a weaker increase in the Weddell Sea, which overcompensate the sea-ice decrease in the WAP region.

The pre-industrial control simulation also shows three climatological low-pressure areas (Figure A.2b) at approximately the same locations as in the reanalysis. However, throughout the entire control simulation neither the observed strength of the ASL nor the observed zonal SLP asymmetry is ever reached. In addition, the modeled ASL is the weakest of the three climatological low-pressure systems. The representation of the ASL is generally poor in current global models (Hosking et al., 2013), which limits the quality of their simulated sea ice. The model additionally overestimates the strength and extent of the coastal easterlies, confining the sea ice at the East

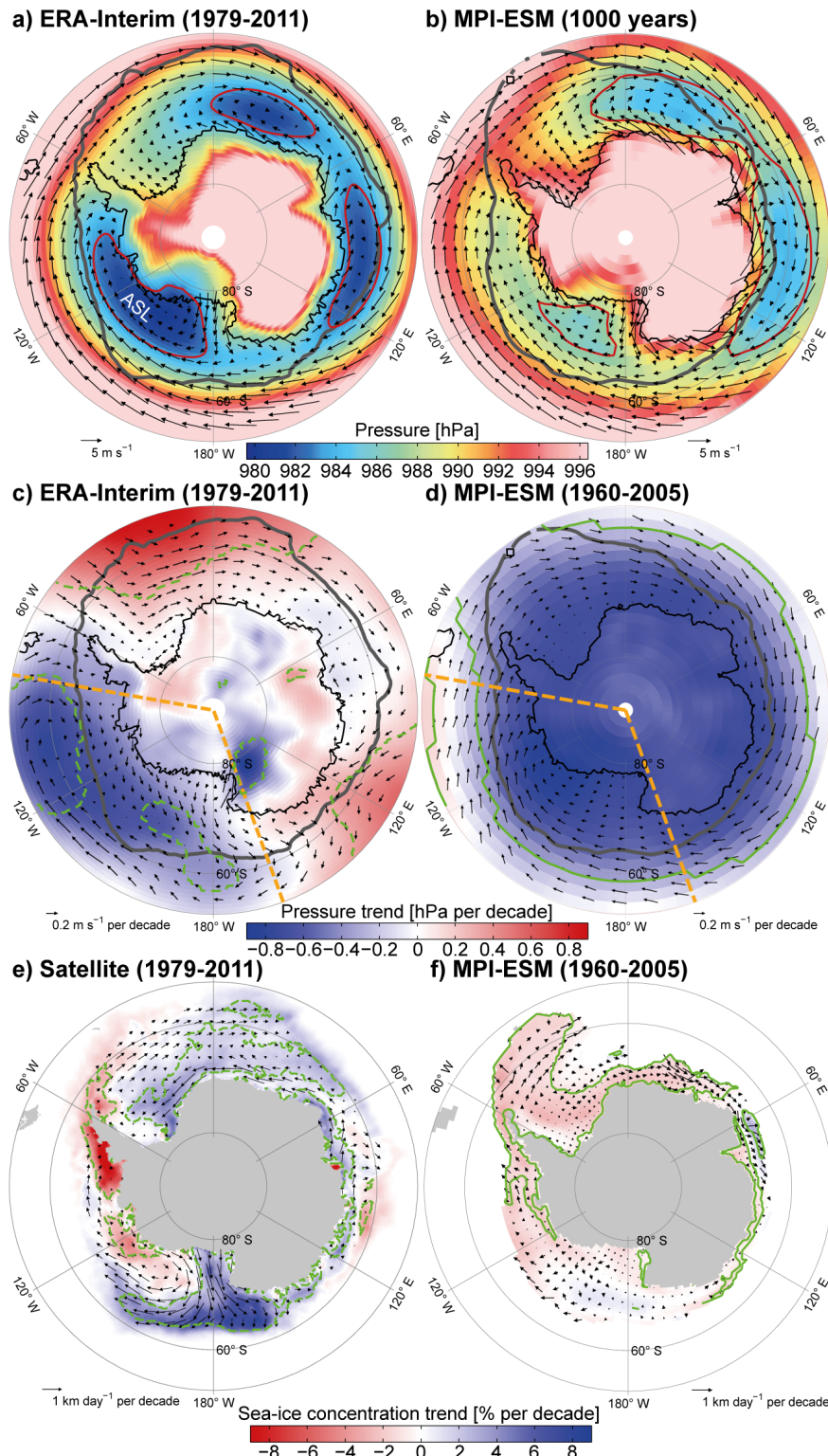


Figure A.2 Annual surface circulation driving Antarctic sea-ice changes: (a) ERA-Interim mean (1979–2011) SLP (shading; red: 983-hPa isobar) and 10-m wind field (vectors). ASL: Amundsen Sea Low. (b) Simulated (pre-industrial) mean SLP (red: 987-hPa isobar) and surface wind field. (c) ERA-Interim decadal SLP and 10-m wind field trends (1979–2011). (d) Simulated decadal SLP and wind field trends (1960–2005, Experiment 1). Black bold lines (a-d): mean annual ice edge. Dashed orange lines (c-d): sector for Figure A.3. (e) Observed (1979–2011) and (f) simulated (1960–2005, Experiment 1) decadal sea-ice concentration (shading) and drift trends (vectors). Dashed and solid green lines: significance of SLP and ice concentration trends (90% confidence level).

Antarctic coast. This rather zonally symmetric circulation is intensified in the historical simulations with all forcings (Experiment 1; 1960–2005; Figure A.2d) due to a statistically significant lowering of the SLP with a somewhat stronger response than the changes in the reanalysis. However, the simulated, zonally almost constant, and poleward shifted SLP lowering causes a westerly to north-westerly wind anomaly everywhere.

The model response (Figure A.2f) does not reproduce the observed sea-ice trends in terms of sign and spatial pattern, which is in line with other models (Turner et al., 2013). The simulated sea-ice changes (1960–2005) are much weaker than the observed ones and amount to an overall decrease. There is a statistically significant ice concentration decrease in the WAP region, in the Weddell Sea, and along the coast of East Antarctica. Also simulated changes in the ice drift are much weaker than observed and rather zonal. This response of the sea ice agrees with the findings by Bitz and Polvani (2012) and Sigmond and Fyfe (2014). They show that in global models increased zonal winds enhance upwelling of warmer water from below that melts the ice. Figure A.2d shows such a westward circulation intensification over most of the sea-ice region, whereas in the ERA-Interim reanalysis intensified westerlies are mostly restricted to the Weddell Sea (Figure A.2c). We conclude that the difference in the observed and simulated sea-ice changes is caused by rather zonal simulated circulation changes and comparably small changes in the meridional winds in the model simulations, which are caused by a weaker asymmetry in the SLP lowering. This also holds if the observational period 1979 to 2011 is analyzed in the model simulation (Figure A.5).

The lowering of the high-latitude SLP leading to the zonal wind intensification in the model most likely results from anthropogenic forcing (Thompson et al., 2011; Lee and Feldstein, 2013). Consequently, we proceed to analyze whether the lowering of the SLP in the ASL region in the reanalysis, thus the sea-ice changes, can also be attributed to these anthropogenic influences. We investigate annual mean geopotential-height changes in vertical cross-sections zonally averaged between 160° E and 80° W (dashed orange lines in Figure A.2c and d). In the reanalysis data (1979–2011), we find three areas of significant (90% confidence level) geopotential-height change (dashed green lines in Figure A.3a). First, the cooling in regions of seasonal ozone depletion in the stratosphere leads to a lowering of the geopotential height there (Thompson et al., 2011). Second, the warming of the troposphere in lower latitudes, most likely caused by the GHG increase, increases the geopotential height there (Santer et al., 2003). As a consequence, the significant lowering of the geopotential height in the high-latitude troposphere is induced by a downward propagation of the stratospheric anomaly from ozone depletion (arrow 1, Figure A.3a), by increasing GHGs and other changes in the external forcing (arrow 2), or by their combination (Lee and Feldstein, 2013).

Our simulations including both GHG increase and stratospheric ozone depletion (Experiment 1, Figure A.3b) show a similar structure and magnitude of the geopotential-height trends (1960–2005) as in ERA-Interim. However, discrepancies occur in the lower troposphere in high

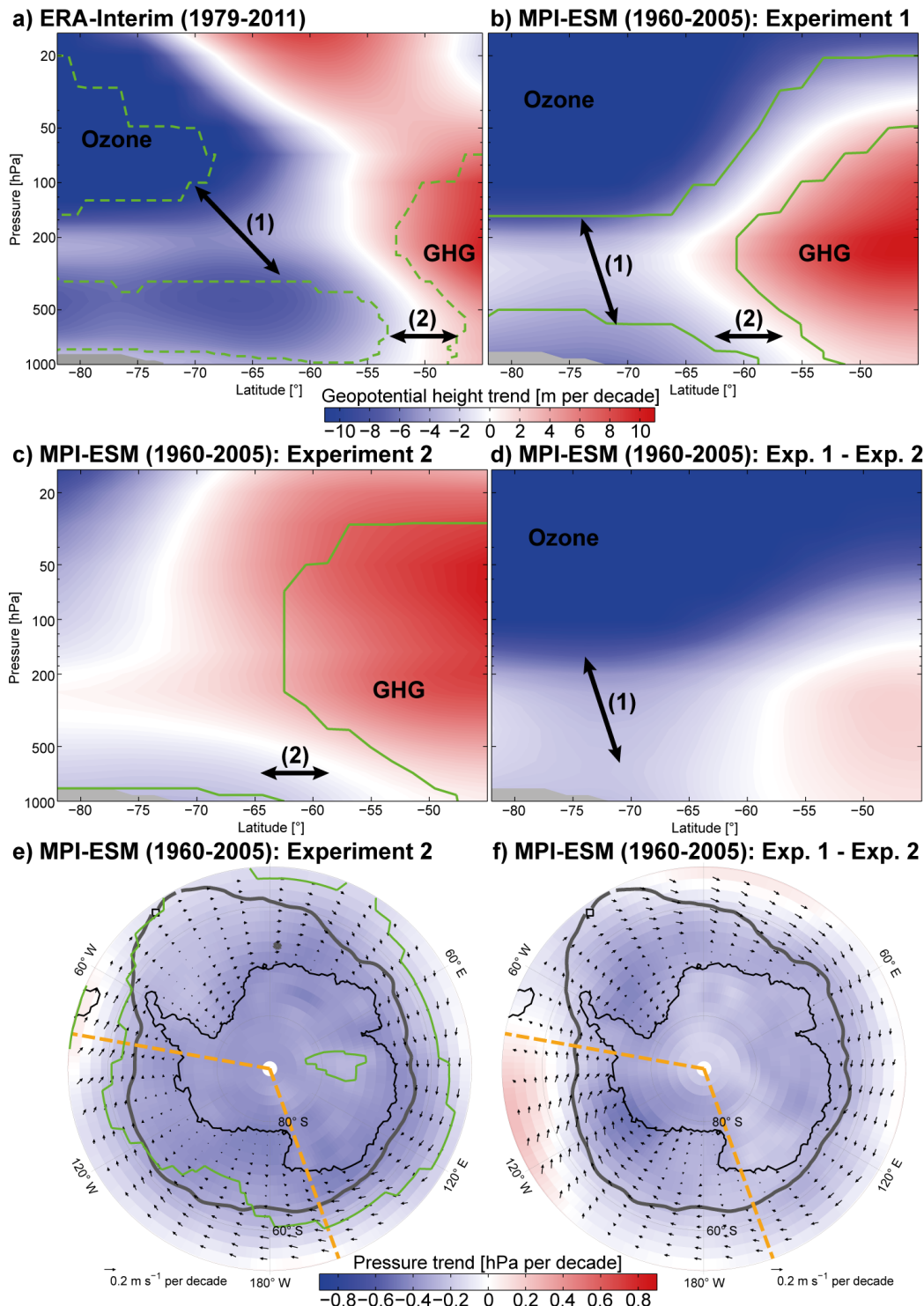


Figure A.3 Attribution of annual surface circulation changes to (1) stratospheric ozone depletion and (2) GHG increase: (a-d) Vertical cross-sections of decadal zonal mean geopotential-height changes between 160° E and 80° W (dashed orange lines in Figure A.2). Experiments as in Figure A.1. (a) ERA-Interim (1979–2011). (b) Simulations with all forcings (1960–2005). (c) Simulations without stratospheric ozone depletion illustrating mainly response to GHG increase (1960–2005). (d) Differences between simulations with (b) and without stratospheric ozone depletion (c) illustrating effect of ozone depletion. (e and f) as (c and d) but for SLP (shading) and surface wind changes (vectors). Dashed orange lines: sector analyzed in (a-d). Black bold lines: mean annual ice edge. Dashed and solid green lines: significance of geopotential-height and SLP trends (90% confidence level).

latitudes (south of 55° S), where modeled trends are slightly weaker, more confined to the surface, and occur at higher latitudes. The simulation with largely constant stratospheric ozone forcing (Experiment 2) results in a significant tropospheric geopotential-height decrease in high latitudes (Figure A.3c), but the trend is much weaker than in the simulation with all forcings (Figure A.3b). The difference of the trends between the two experiments is primarily due to stratospheric ozone depletion (Figure A.3d). Consequently, the SLP trends in the ASL region can mostly be explained by the combined effect of stratospheric ozone depletion and GHG increase (Figure A.3e and f). If we analyze the model output only during the observational period (1979–2011; Figure A.6), the effect of ozone depletion dominates the near-surface changes compared to the GHG increase, which is consistent with previous studies (Thompson et al., 2011; Lee and Feldstein, 2013).

We conclude that the observed SLP lowering in the ASL region and the associated surface circulation changes (Figure A.2c), thus the observed sea-ice trends in this region, are influenced by the combination of anthropogenic ozone depletion and GHG increase, where the signal from ozone depletion presumably dominates. These conclusions are consistent with the suggestions by Turner et al. (2009). We show that the difference in the sea-ice response between global model simulations and observations occurs primarily due to the zonal distribution of the SLP response. A simulated rather zonal circulation intensification leads to a weak overall sea-ice decline, consistent with Bitz and Polvani (2012), while the observed intensified meridional circulation induces strong regional changes and acts to increase the overall sea-ice concentration in the period 1979 to 2011, consistent with Holland and Kwok (2012). In the following, we will discuss whether this difference in the spatial distribution of the changes can be attributed to general shortcomings in the model circulation or to multi-decadal natural variability.

A.4 Discussion

A rather zonally symmetric simulated SLP and circulation response to the anthropogenic forcing, as in our simulations, is a common feature among global models (Son et al., 2010). Yet, this response is not consistent with, for example, observed asymmetric tropospheric geopotential-height changes that have been related to stratospheric ozone depletion (Neff et al., 2008). The observed mean asymmetric circulation (Figure A.2a) is related to orographic blocking effects (Fogt et al., 2012), the asymmetric Antarctic land mass (Lachlan-Cope et al., 2001), and topography-driven boundary layer wind systems (Haumann, 2011). These arguments suggest that the too zonal near-surface circulation in the mean state and also the rather zonal response pattern over the sea ice in global models could be caused by a too smooth topography due to the models' coarse resolution and a not very realistic representation of the Antarctic surface climate. Our findings support this, since the response pattern differs mostly in the high-latitude troposphere in the ASL region (Figure A.2) and the other sectors (40° W to 150° E; Figure A.7).

The Antarctic sea-ice response in global models to zonal wind changes as described by Bitz and Polvani (2012) and Sigmond and Fyfe (2014) is presumably sensitive to the vertical stability of the underlying ocean. In MPI-ESM the high-latitude Southern Ocean vertical stability is underestimated (Stössel et al., 2015), which is a common feature among global models (Heuzé et al., 2013). We hypothesize that a comparably unstable ocean responds with a stronger subsurface heat flux to increasing zonal winds, because the observed changes in the westerly wind component at the ice edge in the Weddell Sea (Figure A.2c) lead to changes in the zonal advection of the ice (Figure A.2e), whereas the westerly anomaly in the model (Figure A.2d) leads to a decreasing ice cover (Figure A.2f). Thus, the underlying mechanism responsible for the simulated sea-ice changes seems to differ from the observed one. Even if the atmospheric circulation response was similar to the observed changes the sea-ice response could still differ from the observations, as it is the case in the Weddell Sea, for example.

Our result that the Antarctic sea-ice response to the anthropogenic influence depends on the asymmetry of the SLP response is in line with the observed response of sea ice to interannual (Fogt et al., 2012; Simpkins et al., 2012) and multi-decadal (Li et al., 2014) variability. These studies show that sea ice changes strongly with the non-annular component of the SAM rather than with the zonally symmetric patterns, where a more positive SAM index is often associated with a lower SLP in the ASL region. However, the spatial structure of the sea-ice changes associated with the positive SAM anomalies during the observational period differs from that of the observed trends (Simpkins et al., 2012). For example, while interannual variations mostly show a change of the strength of the ASL, in the observed trend the ASL additionally expands (see section 3). Abram et al. (2014) show that the SAM shifts to more positive values due to the anthropogenic forcing, which is consistent with both our model simulations and the pressure changes in the ERA-Interim reanalysis since the meridional pressure gradient increases (Figure A.2). However, the effect that this has on the sea ice depends on the zonal structure.

Patterns of sea-ice changes induced by multi-decadal variability in the ASL SLP through connections with the tropics are similar to the observed trends (Li et al., 2014). Consequently, recent changes in the Antarctic sea ice might be influenced by natural variability. A multi-decadal variability in the observed summer-time air temperature records supports such an influence (Fan et al., 2014). Within the 1000-year long control simulation with MPI-ESM about 9% of all possible 968 33-year long periods have an ASL SLP trend larger than the observed trend (averaged over the ocean surface south of 60° S and between 180° E and 80° W). This suggests that the current observed Antarctic sea-ice trends could also be fully explained by natural variability in the SLP and the related wind forcing. In turn, this would be inconsistent with a strong simulated circulation response to the anthropogenic influence. Thus, it is more likely that the observed changes are a mixture of an anthropogenic influence and multi-decadal variations. Yet, we cannot quantify their contributions since neither the pattern of the modeled sea-ice variability, nor that of the modeled response to the forcing currently reproduce the observed pattern of sea-ice trends in coupled models.

Several other mechanisms have been suggested to contribute to the observed Antarctic sea-ice changes. The recent freshening of the Southern Ocean could have increased the sea-ice cover by stabilizing the water column (Bintanja et al., 2013). Goosse and Zunz (2014) suggested that the sea-ice increase is largely driven by a positive ice-ocean feedback that decreases oceanic upwelling and might be initiated by changes in ice advection due to variations in the atmospheric circulation. However, as we show here, there is confidence that the dominant cause of observed sea-ice changes are persisting changes in the atmospheric circulation because the patterns of circulation changes almost perfectly match those of ice drift and concentration in independent data sets over multi-decadal time scales (cf. Figures A.2c and e), confirming the findings by Haumann (2011) and Holland and Kwok (2012). It is possible that these changes in atmospheric circulation cause additional feedbacks through changes in precipitation, oceanic upwelling, or gyre circulation. Atmospheric circulation changes, nevertheless, remain the most likely driver of the observed Antarctic sea-ice changes independent of the question whether multi-decadal variability or anthropogenic forcing is the underlying cause.

A.5 Summary & conclusions

Combining observations with model simulations, we find that the recently observed Antarctic sea-ice changes (1979–2011) are mostly driven by atmospheric circulation changes, which are in turn consistent with at least a partial anthropogenic influence. Satellite and reanalysis data show that intensified meridional winds increase the northward ice advection in the Ross Sea and meridional heat exchange in the Ross Sea and WAP regions, where the largest sea-ice changes are observed. This confirms the findings by Haumann (2011) and Holland and Kwok (2012) for the full observational period. These circulation changes are caused by a significant, zonally asymmetric lowering of the SLP, which is evident as an expansion and strengthening of the ASL.

Our model experiments (MPI-ESM) show that such SLP changes in this region can be explained by a combination of stratospheric ozone depletion and GHG increase (in line with Son et al. (2010)), where the former dominates during the observational period (1979–2011). We conclude that also the observed circulation-driven sea-ice changes are influenced by these anthropogenic forcings (consistent with Turner et al. (2009)). However, similar to other global models (Son et al., 2010), MPI-ESM’s SLP response is rather zonally symmetric leading to a circumpolar westerly wind anomaly and little changes in meridional winds. A too zonally symmetric SLP compared to observations also occurs in the mean state and the natural variability. Thus, we argue that also the response to the anthropogenic influence might lack in zonal asymmetry, which might be caused by the coarse resolution of the Antarctic topography and inaccuracies of the representation of the Antarctic surface climate in the sea-ice area in global models. Consistent with findings by Bitz and Polvani (2012) and Sigmond and Fyfe (2014), this zonal circulation change leads to a weak modeled overall sea-ice decline, whereas regions that experience strengthened

westerlies in the observations (e.g. the Weddell Sea) mostly show a zonal redistribution of the sea ice. We argue that an underestimated vertical stability of the underlying ocean in our model (Stössel et al., 2015) and other global models (Heuzé et al., 2013) might cause this difference. We conclude that most of the discrepancy between the observed and modeled Antarctic sea-ice trends arises from the difference in the zonal distribution of SLP changes and the different sea-ice response to zonal and meridional wind changes.

The model simulates multi-decadal variations of SLP in the ASL region of comparable magnitude to the observed trends. This supports recent suggestions of an influence of multi-decadal variability on observed sea-ice trends (Fan et al., 2014; Li et al., 2014). However, we show that the recent argument that observed sea-ice changes could be purely driven by multi-decadal variability (Polvani and Smith, 2013) is inconsistent with the simulated SLP response to the anthropogenic influence. A clear distinction between effects imposed by natural variability and anthropogenic forcing will only become possible once models accurately represent asymmetries in the near-surface circulation and the associated sea-ice patterns.

Acknowledgments: Model output is available from the authors upon request. We thank U. Mikolajewicz, N. Gruber, H. Haak, E. Olasson, and S. Kern for comments and discussion. We also thank M. van den Broecke, J. Lenaerts, and J. van Angelen for some initial thoughts contributing to this study. This work has primarily been funded through a Max Planck Research-Group fellowship. F.A.H. has been supported by ETH Research Grant CH2-01 11-1. H.S. received funding from the German Research Foundation (DFG) within the research group SHARP under grant SCHM2158/2-2. Computational resources were made available by Deutsches Klimarechenzentrum (DKRZ) through support from the Bundesministerium für Bildung und Forschung (BMBF).

A.6 Supplementary methods

Simulated trends are calculated from 1960 to 2005 and observed trends from 1979 to 2011. We choose a different period for the simulations to obtain a clear forcing response (cf. Figure A.1) and avoid influences of natural variability. However, for consistency, we extend the historical simulations (1850–2005) with the respective RCP4.5 scenario simulations (Giorgetta et al., 2012c) to obtain the model response for the full observation period (until 2011). Figures A.5 and A.6 show that our conclusions are not affected by the different analysis period. At each grid point, we test the trends against internal variability applying a t-test that accounts for a lag-1 temporal auto-correlation. As a measure of internal variability in the observations, the reanalysis data, and the model data, we use the slope’s standard error from the residuals. For the simulated trends, we additionally calculate at each grid point the standard deviation from the total pre-industrial control simulation and the standard deviation from each 46-year interval in the pre-industrial control sim-

ulation. We conservatively take the maximum of these two measures and of the slope's standard error from the residuals as a measure of internal variability.

A.7 Supplementary figures

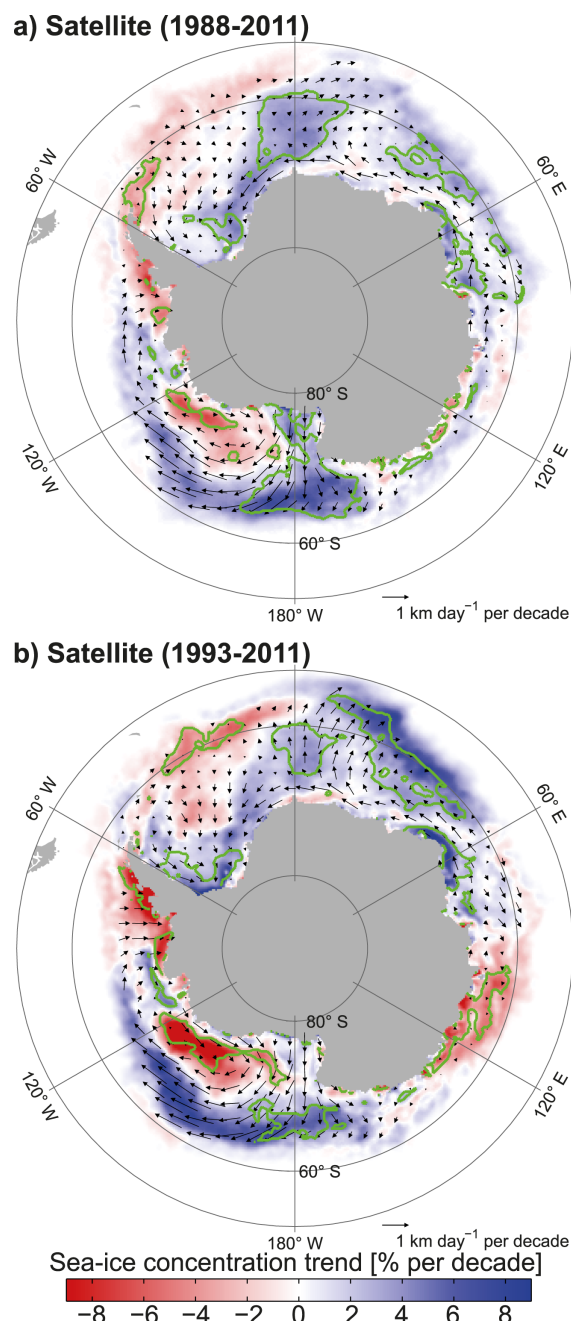


Figure A.4 Observed decadal sea-ice concentration and drift trends for different periods: As Figure A.2e but for the periods 1988 to 2011 and 1993 to 2011 to show that potential inconsistencies in the data set occurring in 1987 and 1992 do not influence the results qualitatively. Prior to 1987 the accuracy of the drift data derived from the SMMR instrument was lower and a potential error in the algorithm parameters in the version 2 of this product could affect the data consistency. After 1992 the availability of the 85 GHz channel improved the accuracy of the drift data (Fowler et al., 2013a).

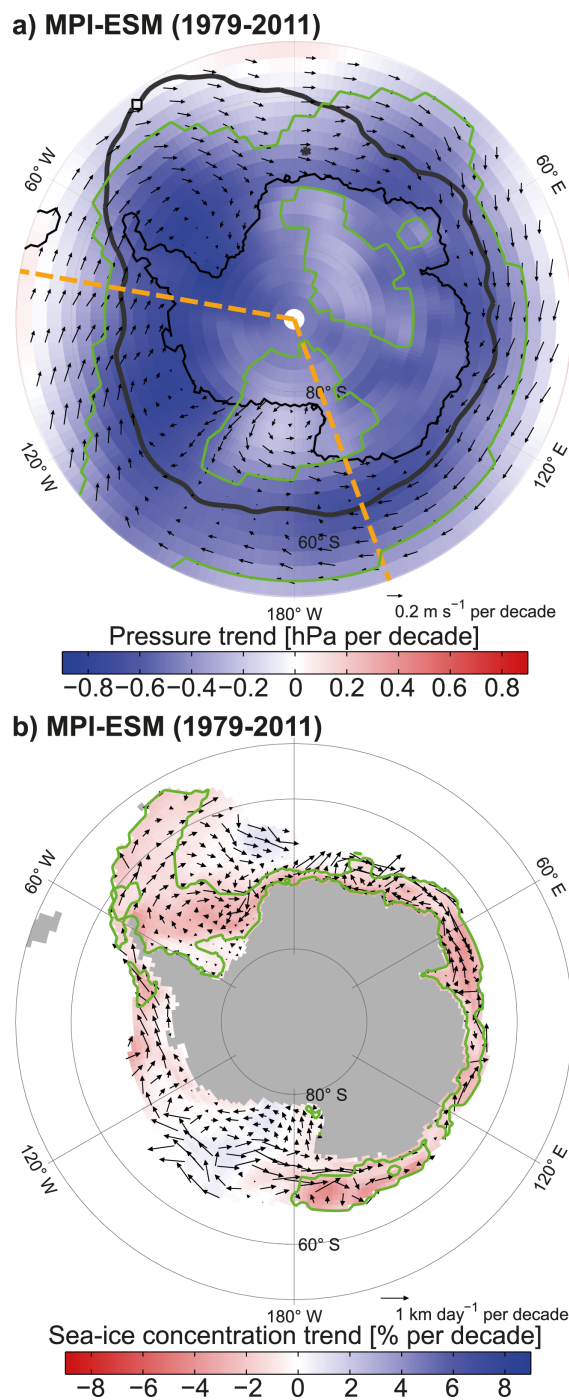


Figure A.5 Simulated decadal atmospheric circulation and sea-ice trends (1979–2011): As Figures A.2d and f but for the period 1979 to 2011 by extending the historical simulation (1979–2005) with the RCP4.5 scenario simulation (2006–2011).

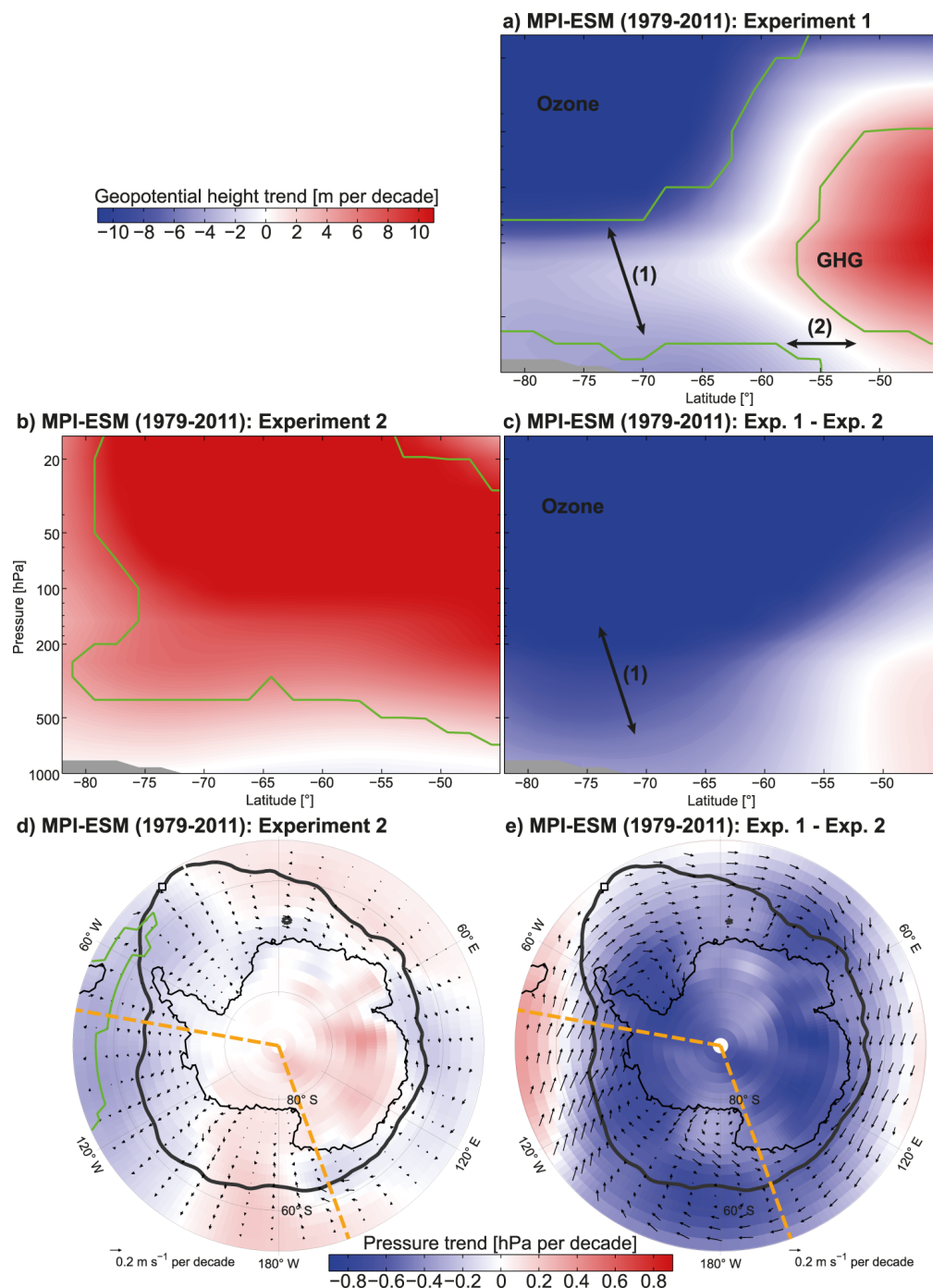


Figure A.6 Attribution of circulation changes to stratospheric ozone depletion and GHG increase (1979–2011): As Figures A.3b through f but for the period 1979 to 2011 by extending the historical simulation (1979–2005) with the RCP4.5 scenario simulation (2006–2011).

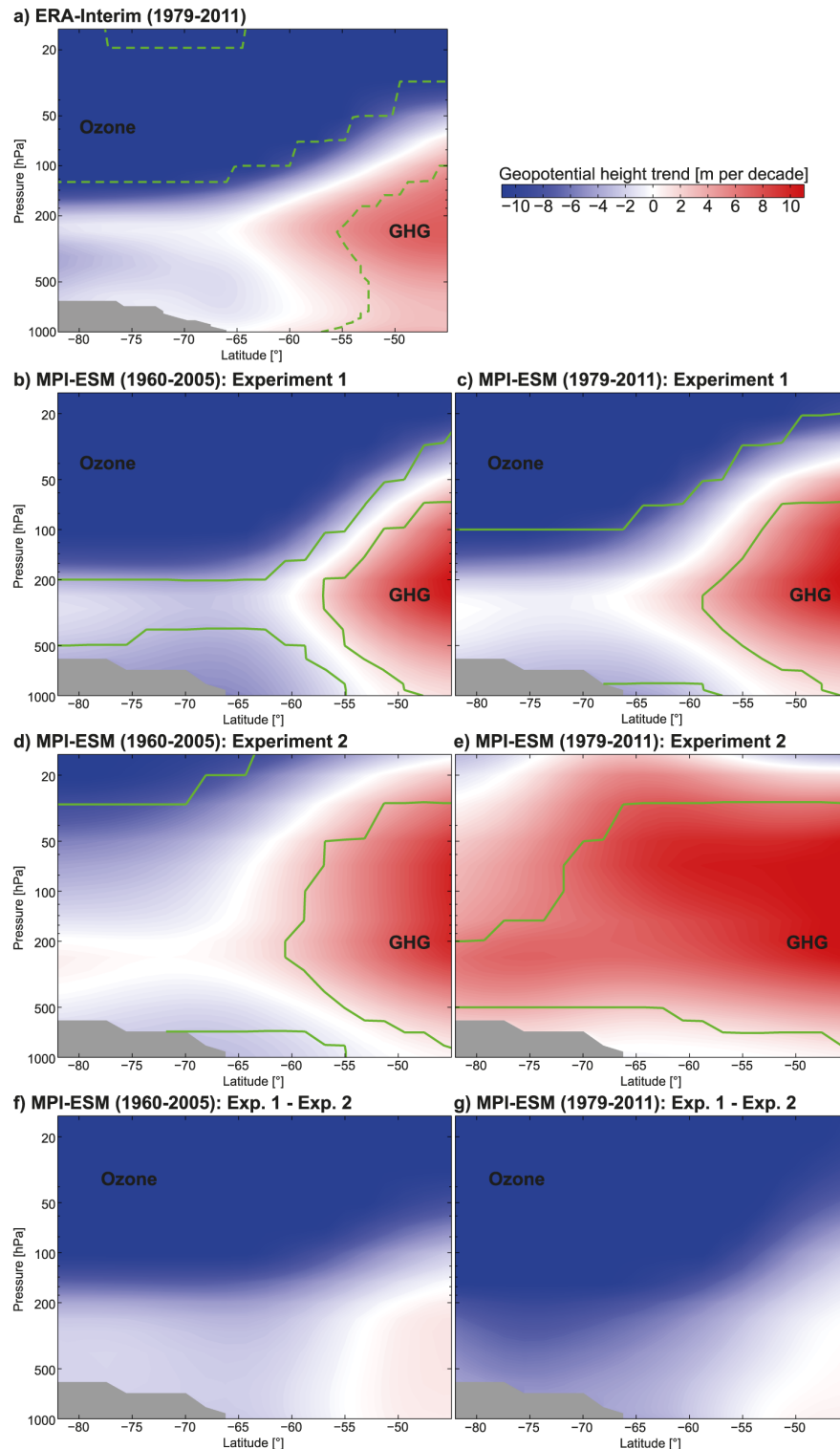


Figure A.7 Vertical cross-sections of decadal zonal mean geopotential-height changes over the sector 40° W to 150° E (based on annual means): Experiments as in Figure A.1. **(a)** ERA-Interim (1979–2011). **(b)** Historical simulations with all forcings (1960–2005). **(c)** Historical+RCP4.5 simulations with all forcings (1979–2011). **(d)** Historical simulations without stratospheric ozone depletion (1960–2005). **(e)** Historical+RCP4.5 simulations without stratospheric ozone depletion (1979–2011). **(f)** Differences between the historical simulations with **(b)** and without stratospheric ozone depletion **(d)** (1960–2005). **(g)** Differences between the historical+RCP4.5 simulations with **(c)** and without stratospheric ozone depletion **(e)** (1979–2011). Dashed and solid green lines: significance of geopotential-height and SLP trends (90% confidence level).